Regular Article

PHYSICAL CHEMISTRY RESEARCH
Published by the
Iranian Chemical Society
www.physchemres.org
info@physchemres.org

***Phys. Chem. Res.**, Vol. 5, No. 4, 643-658, December 2017*
DOI: 10.22036/pcr.2017.75313.1355

Empirical Potential Energy Curve for the Ground State of CaH from a Multi-isotopologue Direct Potential Fit Analysis

A. Shayesteh* and E. Ghazizadeh
School of Chemistry, College of Science, University of Tehran, Tehran 14176, Iran
(Received 31 January 2017, Accepted 25 June 2017)

Vibration-rotation and pure rotational data in the $X^2\Sigma^+$ ground state and electronic data from the $A^2\Pi$-$X^2\Sigma^+$ and $B^2\Sigma^+$-$X^2\Sigma^+$ transitions of CaH and CaD were used in the quantum-mechanical direct-potential-fit (DPF) analysis to determine an analytic potential energy function for the $X^2\Sigma^+$ ground state of CaH, and a radial correction function for the CaD isotopologue. The potential energy function for the $X^2\Sigma^+$ state reproduces all the observed energy levels of CaH and CaD within their experimental uncertainties. In addition, it follows the *ab initio* potential very closely outside the data region, and has the theoretical long-range behavior near the asymptote.

Keywords: Direct-potential-fit, Calcium hydride, Calcium deuteride, MLR potential

INTRODUCTION

Calcium hydride is an important astrophysical molecule [1-3]. It has been identified in the spectra of sunspots, cool stars, M-dwarfs and subdwarfs by its orange and red bands belonging to the $A^2\Pi$-$X^2\Sigma^+$ and $B^2\Sigma^+$-$X^2\Sigma^+$ transitions [4-6]. Studies on the $A^2\Pi$-$X^2\Sigma^+$ and $B^2\Sigma^+$-$X^2\Sigma^+$ transitions of CaH and CaD started early in the 20th century [7-10], and extended significantly in the 1970s [11-14]. The equilibrium electronic energies (T_e) of the $A^2\Pi$ and $B^2\Sigma^+$ state differ by 1350 cm^{-1}, which is almost equal to the vibrational wavenumber of CaH in both states. Thus, all the observed vibrational levels of the $B^2\Sigma^+$ state of CaH (v_B = 0, 1, 2) are perturbed [11] by those of the $A^2\Pi$ state (v_A = 1, 2, 3), but the vibrational levels of CaD are not perturbed [15].

Spectroscopic studies on CaH and CaD prior to 1976 have been listed in Huber and Herzberg's book [16], which includes several electronic transitions involving the $X^2\Sigma^+$ ground state and the $A^2\Pi$, $B^2\Sigma^+$, $C^2\Sigma^+$, $D^2\Sigma^+$, $E^2\Pi$ and higher-lying electronic states [16–20]. The $A^2\Pi$ and $B^2\Sigma^+$ states of CaH were studied again by laser spectroscopy [21], and the $D^2\Sigma^+$-$X^2\Sigma^+$ spectra for both CaH and CaD were recorded by Bell *et al.* [22] and Gustavsson *et al.* [23]. Martin generated empirical potential energy curves for the $X^2\Sigma^+$, $B^2\Sigma^+$ and $D^2\Sigma^+$ states using spectroscopic data from both CaH and CaD [24]. Recently, high resolution Fourier transform emission spectra of the $E^2\Pi$-$X^2\Sigma^+$ transitions of CaH and CaD have been analyzed [25].

Steimle and co-workers studied the $A^2\Pi$-$X^2\Sigma^+$ and $B^2\Sigma^+$-$X^2\Sigma^+$ transitions of CaH and CaD using laser-induced fluorescence [26]. They measured low-J lines in the presence of magnetic or electric fields [27-29], and determined permanent electric dipole moments for the $X^2\Sigma^+$, $A^2\Pi$ and $B^2\Sigma^+$ states. Due to the appearance of these electronic transitions in solar and stellar spectra, the $A^2\Pi$-$X^2\Sigma^+$ and $B^2\Sigma^+$-$X^2\Sigma^+$ emission spectra of CaH and CaD were recorded recently by Bernath and co-workers [30,31] at high temperatures using a Fourier transform spectrometer, and spectroscopic constants were obtained for the $A^2\Pi$ and $B^2\Sigma^+$ states of both isotopologues. High vibrational levels in the double-minimum $B^2\Sigma^+$ state were measured very recently by laser-induced fluorescence [32].

Calcium hydride has been the subject of several *ab initio* calculations, which focused mainly on potential energy curves of the low-lying electronic states, and the dipole moments of the $X^2\Sigma^+$, $A^2\Pi$ and $B^2\Sigma^+$ states [33-39]. Pure

*Corresponding author. E-mail: ashayesteh@ut.ac.ir

theoretical line lists with oscillator strengths have been computed for the $A^2\Pi$- $X^2\Sigma^+$ and $B^2\Sigma^+$-$X^2\Sigma^+$ transitions by Weck *et al*. [40], although their theoretical line positions do not match experimental data, and discrepancies of ~10 cm^{-1} exist for some vibrational wavenumbers.

Spectroscopic measurements within the $X^2\Sigma^+$ ground state of CaH began in 1989, when Petitprez *et al*. recorded diode laser infrared spectra, and observed vibrational levels up to v = 4 for both CaH and CaD isotopologues [41]. Fourier transform infrared emission spectra of CaH were recorded [42,43], and CaH vibrational levels up to v = 4 were measured. Accurate rotational constants for the v = 0 of CaH and CaD in the $X^2\Sigma^+$ ground state have been determined from millimeter-wave spectra [44,45]. Shayesteh *et al*. combined their infrared data with all ground state data available in the literature, and obtained Dunham constants for the $X^2\Sigma^+$ state using a multi-isotopologue fit [43].

In the present study, we have collected the available pure rotational, vibration-rotation and electronic data for the $X^2\Sigma^+$, $A^2\Pi$ and $B^2\Sigma^+$ states of CaH and CaD, and used the quantum-mechanical direct-potential-fit (DPF) method to determine an analytic potential energy function for the $X^2\Sigma^+$ ground state. This potential energy function incorporates the theoretically known long-range behavior, and reproduces all the observed energy levels of CaH and CaD within their experimental uncertainties.

DATA USED IN THE ANALYSIS

The present work is an analysis of the data from pure rotational, vibration-rotation and electronic spectra of ^{40}CaH and ^{40}CaD. Barclay *et al*. [44] recorded the millimeter-wave spectra in absorption, including the N = 1 ← 0 rotational transition of ^{40}CaH and the N = 1 ← 0 to 3 ← 2 rotational transitions of ^{40}CaD with uncertainties of $\pm 10^{-6}$ cm^{-1}. Frum *et al*. [45] measured the N = 1 ← 0 and 2 ← 1 rotational transitions for ^{40}CaH and N = 3 ← 2 to 5 ← 4 for ^{40}CaD with uncertainties of $\pm 10^{-5}$ cm^{-1}. The diode laser infrared spectra of CaH and CaD, recorded by Petitprez et al. [41], contained the v = 1 ← 0 to 4 ← 3 bands of both isotopologues in the $X^2\Sigma^+$ ground state with uncertainties of ±0.001 cm^{-1}. Shayesteh *et al*. [43] recorded Fourier transform infrared emission spectrum of CaH, and measured the v = 1 ← 0 to 4 ← 3 bands with uncertainties of ±0.001 cm^{-1}. They included all previous ground state data in their fits, and for the pure rotational lines, they calculated hyperfine-free line positions. We took all ground state data from Ref. [43], and added new data from electronic transitions of CaH and CaD [30,31] to our data set.

Compared to the infrared data, the $A^2\Pi$-$X^2\Sigma^+$ and $B^2\Sigma^+$-$X^2\Sigma^+$ transitions of CaH and CaD, recorded recently by Bernath and co-workers [30,31], span a much larger range of J values. We thus included all their data in our data set. Lines from the Δv = 0 sequence in both $A^2\Pi$-$X^2\Sigma^+$ and $B^2\Sigma^+$-$X^2\Sigma^+$ transitions of CaH have uncertainties of ±0.003 cm^{-1}, while for CaD and the other sequences of CaH, typical uncertainties are ±0.005 cm^{-1}. The electronic data of Bernath and co-workers [30,31] span v = 0 to 4 of the $X^2\Sigma^+$ ground state for both CaH and CaD. We also noted that in some emission bands in the $D^2\Sigma^+$-$X^2\Sigma^+$ transition of CaD isotopologue, Gustavsson [23] had observed the v = 5, 6 and 7 levels of the ground state, and their vibrational energies and rotational constants were later reported in Martin's paper [24]. We included these vibrational energies and rotational constants for CaD with uncertainties of ±0.1 and ±0.001 cm^{-1}, respectively. An overview of all the data used in our analysis is presented in Table 1.

DIRECT-POTENTINAL-FIT DATA ANALYSIS

The Radial Hamiltonian and Potential Energy Function

In the "direct-potential-fit" (DPF) analysis, the parameters of an analytic potential energy function are fitted directly to the differences between observed energy level spacings and eigenvalues obtained by solving the radial Schrödinger equation. For a neutral diatomic molecule with a closed-shell electronic structure, the radial equation is [46-52]:

$$-\frac{\hbar^2}{2\mu}\left[1+g_\beta(r)\right]\frac{d^2\psi_{v,J}(r)}{dr^2}+\left\{V_{CN}(r)+\Delta V_{ad}(r)+\frac{\hbar^2 J(J+1)}{2\mu r^2}\left[1+g_\omega(r)\right]\right\}\psi_{v,J}(r)=E_{v,J}\psi_{v,J}(r) \quad (1)$$

in which μ is the reduced mass and $V_{CN}(r)$ is the "clamped nuclei" electronic potential, and $\Delta V_{ad}(r)$ is the adiabatic

Table 1. Experimental Data Used in the Present Study

Isotopologue	Transition	unc. (cm^{-1})	v'	v''	No. Data	Ref.
^{40}CaH	Pure rotational	$\pm10^{-6}$	-	0	2	[44]
	Pure rotational	$\pm10^{-5}$			4	[45]
	Infrared	±0.001	-	0-4	504	[43]
	$A^2\Pi\rightarrow X^2\Sigma^+$	±0.003	0-3	1-4	1294	[30]
	$A^2\Pi\rightarrow X^2\Sigma^+$	±0.005	0-3	1-4	1301	[30]
	$B^2\Sigma^+\rightarrow X^2\Sigma^+$	±0.003	0-2	0-2	385	[30]
	$B^2\Sigma^+\rightarrow X^2\Sigma^+$	±0.005	2	3	33	[30]
	$B^2\Sigma^+\rightarrow X^2\Sigma^+$	±0.1	1,2	0,1	139	[21]
^{40}CaD	Pure rotational	$\pm10^{-6}$	-	0	4	[44]
	Pure rotational	$\pm10^{-5}$	-	0	6	[45]
	Infrared	±0.001	-	0-4	128	[41]
	$A^2\Pi\rightarrow X^2\Sigma^+$	±0.005	0-2	0-3	2055	[31]
	$A^2\Pi\rightarrow X^2\Sigma^+$	±0.01	3	3,4	303	[31]
	$B^2\Sigma^+\rightarrow X^2\Sigma^+$	±0.005	0-2	0-2	632	[31]
	$D^2\Sigma^+\rightarrow X^2\Sigma^+$	±0.1	0-4	5-7	6	[24]

contribution to the potential, which is isotope-dependent. The terms $g_\beta(r)$ and $g_\alpha(r)$ take account of non-adiabatic corrections to the radial and angular kinetic energy operators, respectively. In order to solve Eq. (1) directly by conventional Numerov-Cooley wavefunction propagation methods, it is common to multiply it by the factor $[1 + g_\beta(r)]^{-1}$, which is then expanded utilizing the fact that $|g_\beta(r)| << 1$. With some more manipulations [49-53] and by taking the potential function of one isotopologue as reference, the following effective radial Schrödinger equation is obtained:

$$\left[-\frac{\hbar^2}{2\mu_i}\frac{d^2}{dr^2}+\left[V_{\rm ad}^{(1)}(r)+\Delta V_{\rm ad}^{(i)}(r)\right]+\frac{\hbar^2 J(J+1)}{2\mu_i r^2}\left[1+g^{(i)}(r)\right]\right]\psi_{v,J}(r)=E_{v,J}\psi_{v,J}(r)\text{,} \quad (2)$$

in which $V_{\rm ad}^{(1)}(r)$ is the total effective internuclear potential at $J = 0$, including all corrections for the selected reference isotopologue. The nonadiabatic centrifugal-potential correction, $g^{(i)}(r)$, is an effective correction function that is approximately equal to $[g_\alpha(r) - g_\beta(r)]$, and is isotope-dependent [49-56]. Therefore, $\Delta V_{\rm ad}^{(i)}(r)$ is only the difference between the effective radial potential (at $J = 0$) for isotopologue i and that of the reference species ($i = 1$). For practical work, *i.e.*, fitting the potential energy functions to experimental data, Eq. (2) is appropriate, and has been implemented in Le Roy's dPotFit program [57]. For a $^2\Sigma^+$ electronic state with rotational quantum number N, Eq. (2) is rewritten as:

$$\left[-\frac{\hbar^2}{2\mu_i}\frac{d^2}{dr^2}+\left[V_{\rm ad}^{(1)}(r)+\Delta V_{\rm ad}^{(i)}(r)\right]+\frac{\hbar^2 N(N+1)}{2\mu_i r^2}\left[1+g^{(i)}(r)\right]+{\rm sg}_\Sigma(e/f;N)\Delta V_\Sigma^{(i)}(r)\right]\psi_{v,N}(r), = E_{v,N}\psi_{v,N}(r) \tag{3}$$

in which $\Delta V_\Sigma^{(i)}(r)$ is the radial strength function for the spin-rotation doubling in isotopologue i, and ${\rm sg}_\Sigma(e/f;N)$ is equal to $+\frac{1}{2}N$ and $-\frac{1}{2}(N+1)$ for the e and f levels, respectively [58].

The Morse-long-range (MLR) model [59,60] was used for the effective adiabatic potential of the $X^2\Sigma^+$ ground state:

$$V_{\rm MLR}(r)=D_{\rm e}\left[1-\frac{u_{\rm LR}(r)}{u_{\rm LR}(r_{\rm e})}\exp\left(-\beta(r).y_p^{\rm eq}(r)\right)\right]^2, \tag{4}$$

in which $D_{\rm e}$ is the equilibrium dissociation energy, $r_{\rm e}$ is the equilibrium internuclear distance, and $u_{\rm LR}(r)$ is the long-range potential. The exponent coefficient $\beta(r)$ is defined by the following equation,

$$\beta(r)=\beta_{p,q}^{\rm ref}(r)=y_p^{\rm ref}(r)\beta_\infty+[1-y_p^{\rm ref}(r)]\sum_{i=0}^{N_\beta}\beta_i y_q^{\rm ref}(r)^i, \tag{5}$$

in which $y_p^{\rm ref}(r)$ and $y_q^{\rm ref}(r)$ are slowly varying functions of the internuclear distance [61]:

$$y_p^{\rm ref}(r)=\frac{r^p-r_{\rm ref}^p}{r^p+r_{\rm ref}^p}. \tag{6}$$

The power p (or q) is usually a small positive integer, and it is possible to choose different values for p and q in Eq. (5) for $\beta(r)$. The reference distance for the expansion ($r_{\rm ref}$) is sometimes set equal to $r_{\rm e}$, *e.g.* in $y_p^{\rm eq}(r)$ of Eq. (4), but in general it can be any chosen internuclear distance. As $r\to\infty$, $y_p^{\rm ref}(r)\to+1$, and the value of β_∞ in Eq. (5) becomes:

$$\beta_\infty\equiv\ln\left[2D_{\rm e}/u_{\rm LR}(r_{\rm e})\right], \tag{7}$$

resulting in the following potential at long-range [62]:

$$V_{\rm MLR}(r)\approx D_e-u_{\rm LR}(r)+u_{\rm LR}(r)^2/4D_e\ . \tag{8}$$

We used the "damped" long-range potential for the CaH molecule:

$$u_{\rm LR}(r)=D_6(r)\frac{C_6}{r^6}+D_8(r)\frac{C_8}{r^8}. \tag{9}$$

The damping functions $D_6(r)$ and $D_8(r)$ in Eq. (9) are the generalized Douketis-type functions [63,64] with s = -1:

$$D_m^{(s)}(r)=\left\{1-\exp\left(-\frac{b^{(s)}(\rho r)}{m}-\frac{c^{(s)}(\rho r)^2}{m^{1/2}}\right)\right\}^{m+s}, \tag{10}$$

in which the two system-independent parameters are $b^{(-1)}$ = 3.30 and $c^{(-1)}$ = 0.423. The system-dependent scaling parameter ρ was calculated to be 0.74 for CaH: $\rho=\rho_{\rm CaH}=2\rho_{\rm Ca}\rho_{\rm H}/(\rho_{\rm Ca}+\rho_{\rm H})$ with $\rho_{\rm H}$ = 1 and $\rho_{\rm Ca}=({\rm IP}^{\rm Ca}/{\rm IP}^{\rm H})^{2/3}$. The values of C_6 and C_8 for the ground state of CaH were taken from Ref. [65].

The Born-Oppenheimer breakdown (BOB) radial functions, $\Delta V_{\rm ad}^{(i)}(r)$ and $g^{(i)}(r)$, are usually written as a sum of two terms, one for each component atom [53,54]. Taking CaH as the reference isotopologue and having BOB corrections only for the hydrogen atom, the BOB functions are simplified to:

$$\Delta V_{\rm ad}^{\rm (CaD)}(r)=\left(\frac{M_{\rm D}-M_{\rm H}}{M_{\rm D}}\right)\widetilde{S}_{\rm ad}^{\rm H}(r) \tag{11}$$

$$g^{\rm (CaH)}(r)=\widetilde{R}_{\rm na}^{\rm H}(r) \tag{12a}$$

$$g^{\rm (CaD)}(r)=\left(\frac{M_{\rm H}}{M_{\rm D}}\right)\widetilde{R}_{\rm na}^{\rm H}(r) \tag{12b}$$

The radial strength functions $\widetilde{S}_{\rm ad}^{\rm H}(r)$ and $\widetilde{R}_{\rm na}^{\rm H}(r)$ are expanded using expressions in which their values at $r_{\rm e}$ and at the potential asymptote are explicit parameters of the MLR model:

$$\widetilde{S}_{\rm ad}^{\rm H}(r)=u_\infty^{\rm H}y_{p_{\rm ad}}^{\rm eq}(r)+[1-y_{p_{\rm ad}}^{\rm eq}(r)]\sum_{i=0}^{N_{\rm ad}^{\rm H}}u_i^{\rm H}y_{q_{\rm ad}}^{\rm eq}(r)^i, \tag{13}$$

$$\widetilde{R}_{\rm na}^{\rm H}(r)=t_\infty^{\rm H}y_{p_{\rm na}}^{\rm eq}(r)+[1-y_{p_{\rm na}}^{\rm eq}(r)]\sum_{i=0}^{N_{\rm na}^{\rm H}}t_i^{\rm H}y_{q_{\rm na}}^{\rm eq}(r)^i. \tag{14}$$

$\widetilde{S}_{\rm ad}^{\rm H}(r)$ is usually given in units of wavenumbers, and $\widetilde{R}_{\rm na}^{\rm H}(r)$ is dimensionless. We adopt Watson's convention [55] of fixing $t_0^{\rm H} = 0.0$, and we also have $u_0^{\rm H} = 0.0$ for the ground state of CaH. In addition, since we choose to set the zero of energy at the energy of separated ground-state atoms, the limiting asymptotic values of these parameters are $u_\infty^{\rm H} = t_\infty^{\rm H} = 0.0$.

Finally, the function $\Delta V_\Sigma^{(i)}(r)$ for the spin-rotation interaction in Eq. (3) is defined as [58]:

$$\Delta V_\Sigma^{(i)}(r) = \left(\frac{\hbar^2}{2\mu_i r^2}\right) f_\Sigma(r), \tag{15}$$

in which $f_\Sigma(r)$ is a simple polynomial in the dimensionless radial variable $y_{q_\Sigma}^{\rm eq}(r)$:

$$f_\Sigma(r) = \sum_{i=0}^{N_\Sigma} w_i^\Sigma y_{q_\Sigma}^{\rm eq}(r)^i. \tag{16}$$

The magnitude of the dimensionless radial function $f_\Sigma(r)$ at the equilibrium distance (r_e) is equal to the ratio of the spin-rotation interaction constant (γ_e) to the inertial rotational constant (B_e).

Data Analysis Procedure

In the first step, we used the Dunham $Y_{l,0}$ and $Y_{l,1}$ coefficients from Ref. [43] to generate RKR potential [66] for the $X^2\Sigma^+$ ground state of CaH. Since the direct-potential-fit procedure is based on nonlinear least-squares fitting and requires relatively accurate starting parameters, the RKR turning points were fitted to MLR potential functions with various values of p, q and $r_{\rm ref}$ using the program BetaFit [67]. The output parameters (β_i) from program BetaFit were used as the starting parameters for the dPotFit program [57]. Since the rotational levels of the $A^2\Pi$ and $B^2\Sigma^+$ excited states of CaH are perturbed, all the observed levels of the $A^2\Pi$ and $B^2\Sigma^+$ states were fitted as independent term values. The quality of the fit is quantified by the value of the dimensionless root-mean-square deviation (DRMSD) [62], which should be close to unity for a good fit [68].

RESULTS AND DISCUSSION

Spectroscopic data considered here span less than half of the ground state well depth, and it is not possible to determine an accurate value for the dissociation energy from the data. Huber and Herzberg [16] reported 14360 cm^{-1} as an upper limit for the equilibrium dissociation energy (D_e) of the $X^2\Sigma^+$ ground state, from predissociation data of the $C^2\Sigma^+$ excited-state. Kerkines and Mavridis [39] obtained an *ab initio* value of 14270 cm^{-1} from relativistic CCSD(T) calculations with uncontracted quintuple-zeta basis sets. Recently, in another *ab initio* study, a value of 14330 cm^{-1} was obtained from multi-reference configuration interaction (MRCI) calculations [69]. We decided to fix the dissociation energy (D_e) at 14300 cm^{-1}, to be consistent with all three values mentioned above. We used the Morse-long-range (MLR) model for the effective adiabatic potential function of the ground state because of its proper description of the short- and long-range behaviors. The numerical values of C_6 and C_8 constants were taken from the article of Mitroy and Zhang [65].

Since there is no experimental information about the $X^2\Sigma^+$ state potential in the region beyond the inner (1.62 Å) and outer (2.65 Å) turning points of the highest observed vibrational level ($v'' = 4$), we added several *ab initio* values for the potential energy curve from MRCI calculations [69]. The *ab initio* points were outside the data region from r = 1.1 to 1.6 Å for the short range, and from r = 2.8 to 4.4 Å for the long range; uncertainties of about 2% were assigned for the *ab initio* points. This constraint imposes physically correct behavior on the short-range repulsive and outer wall attractive parts of the resulting fitted potential.

Generally, the dimensionless-root-mean-square deviation (DRMSD) of the fit varies with the order of the MLR exponent polynomial N_β and the location of expansion centre $r_{\rm ref}$ for different values of the expansion coefficient powers p and q. We used $r_{\rm ref}$ values from 2.60 to 2.90 Å, in 0.05 Å intervals, and obtained a series of fits for different values of $p = q$ = 3, 4 or 5 with N_β = 7 or 8. Figure 1 summarizes the results obtained for the six potential functions at seven different $r_{\rm ref}$ values. In order to minimize DRMSD with the smallest possible number of parameters, the best radial function $\beta(r)$ for the MLR potential was chosen to be the one with N_β = 7, $p = q$ = 4, and $r_{\rm ref}$ = 2.75 Å. It has been reported previously that when *ab initio* points are added, it is possible to have $r_{\rm ref}$ values larger than the outer turning point of the highest observed vibrational level

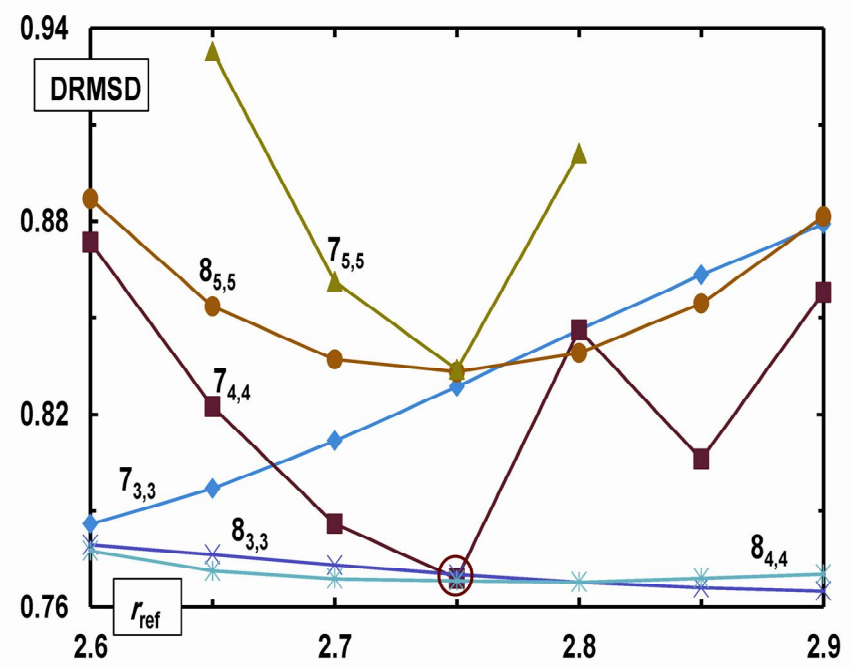

Fig. 1. Dependence of DRMSD on the exponent polynomial order N_β and the expansion center location r_{ref} for expansion function variables defined by $\{p,q\}$ = {3,3}, {4,4} and {5,5} in the MLR potential energy function fits for the $X^2\Sigma^+$ ground state of CaH.

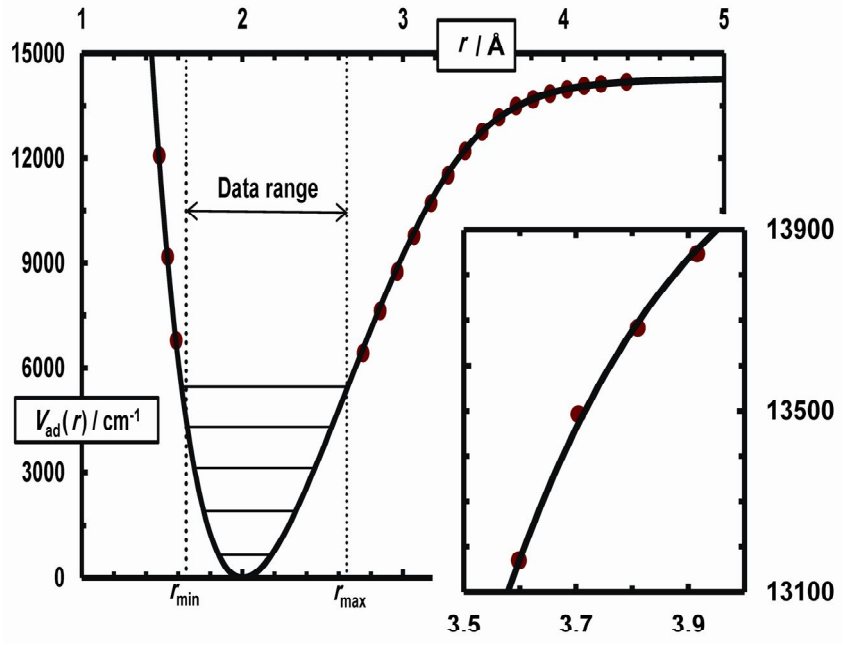

Fig. 2. Plot of potential energy function determined for the $X^2\Sigma^+$ ground state of CaH, with energy levels indicating the experimental data. The circles are the ab initio points of Ref. [69].

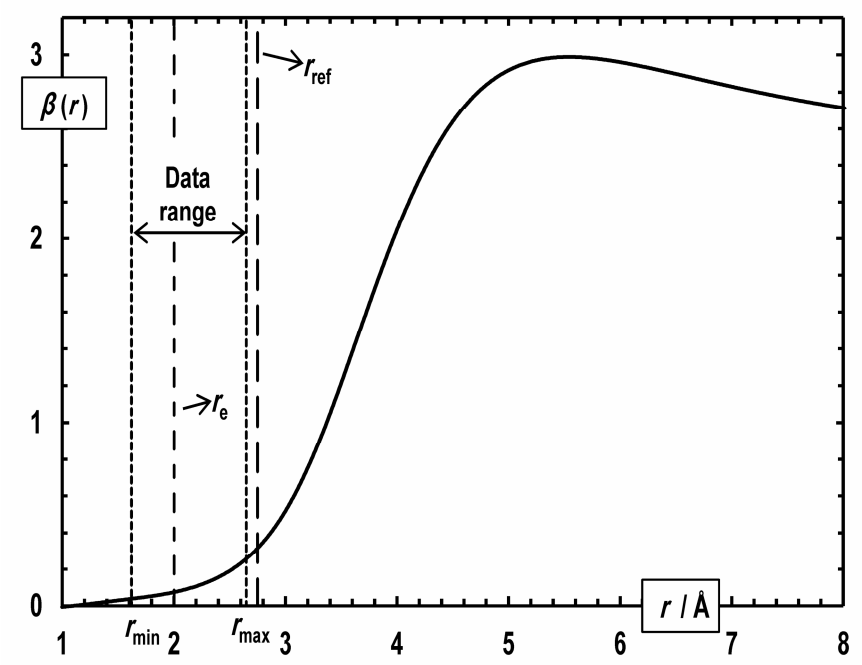

Fig. 3. Plot of the distance-dependent exponent coefficient function for the $X^2\Sigma^+$ state of CaH.

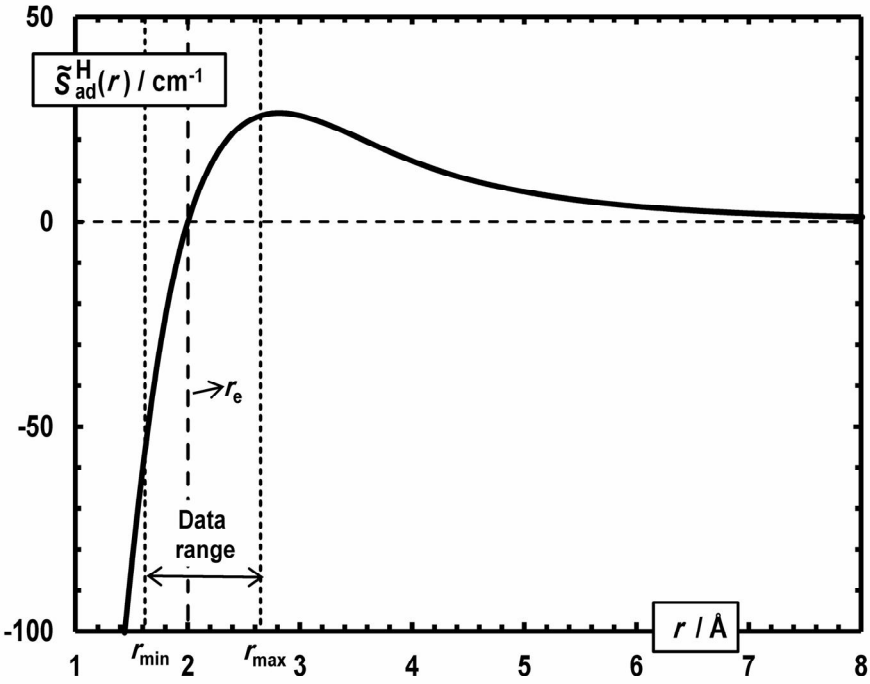

Fig. 4. Plot of the fitted H-atom adiabatic radial BOB function determined for the $X^2\Sigma^+$ state of CaH.

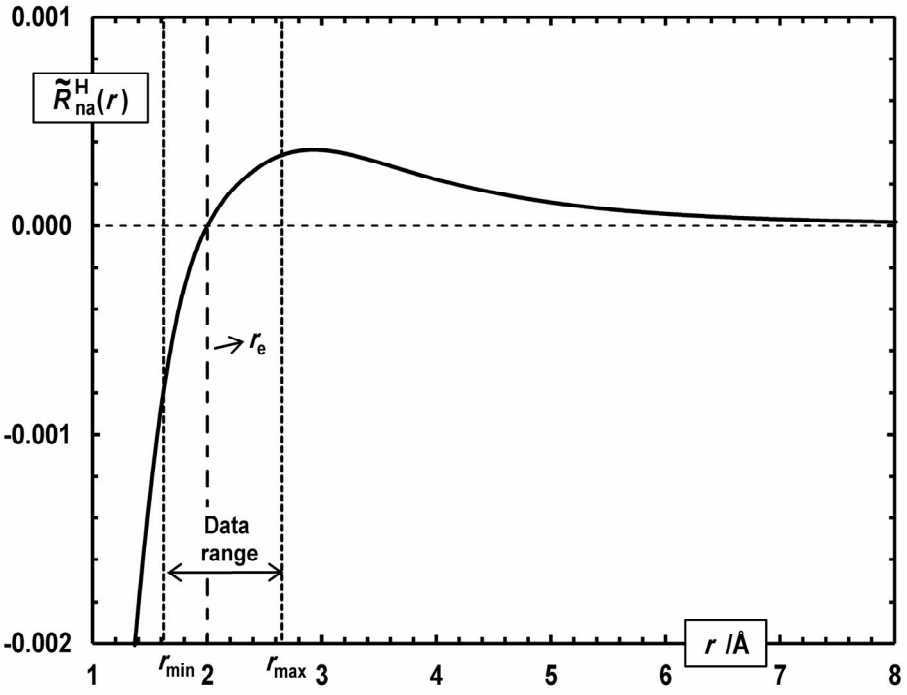

Fig. 5. Plot of the fitted H-atom non-adiabatic centrifugal BOB function determined for the $X^2\Sigma^+$ state of CaH.

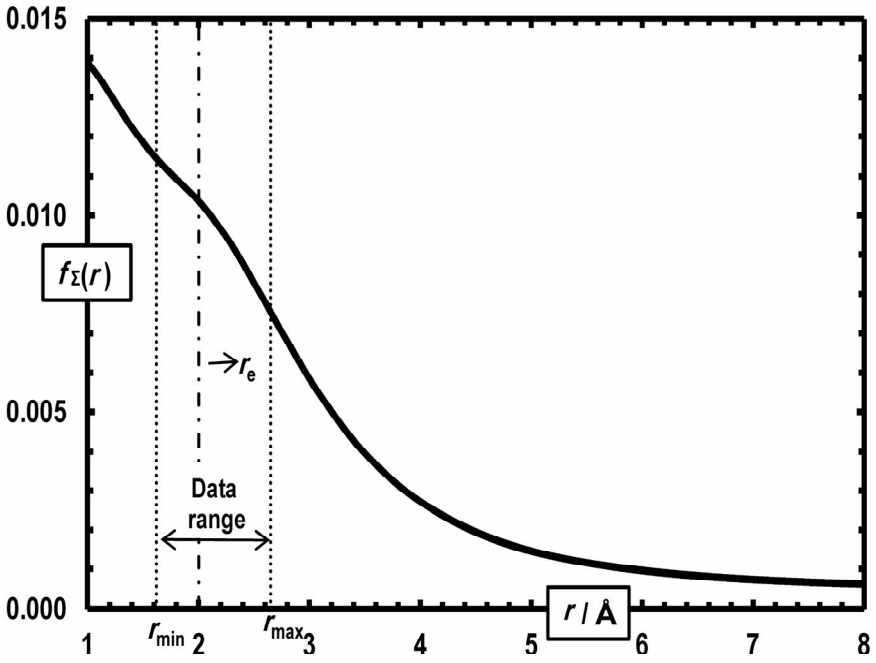

Fig. 6. Plot of the spin-rotation doubling radial strength function determined for the $X^2\Sigma^+$ state of CaH.

Table 2. Parameters Defining the Recommended MLR Potential Energy Function for the $X^2\Sigma^+$ State and the Associated BOB and Spin-rotation Doubling Functions, as Determined from the DPF Analysis. The Long-range Potential Incorporates the Generalized Douketis-type Damping Functions with $s = -1$ and $\rho_{CaH} = 0.74$

MLR potential parameters	$X^2\Sigma^+$	Correction parameters	$X^2\Sigma^+$
T_e (cm^{-1})	0.0	$\{p_{ad}, q_{ad}\}$	{4, 4}
D_e (cm^{-1})	14300 (Fixed)	u_1^H (cm^{-1})	88.567(29)
r_e (Å)	2.0023637(2)	u_2^H (cm^{-1})	-6.16(6)
C_6 (cm^{-1} Å^6)	4.824×10^5	u_3^H (cm^{-1})	62.0(21)
C_8 (cm^{-1} Å^8)	8.504×10^6	u_4^H (cm^{-1})	16.7(17)
$\{p, q\}$	{4, 4}	$\{p_{na}, q_{na}\}$	{4, 4}
r_{ref} (Å)	2.75	t_1^H	0.0010389(110)
β_0	0.32135341(2700)	t_2^H	-0.00026(10)
β_1	-1.3542224(1400)	t_3^H	0.00171(6)
β_2	0.047742(1700)		
β_3	1.83695(970)	$\{q_\Sigma\}$	{4}
β_4	3.53096(3000)	w_0^Σ	0.0103508(38)
β_5	4.0791(490)	w_1^Σ	-0.00312(9)
β_6	2.794(42)	w_2^Σ	-0.00265(29)
β_7	0.864(14)	w_3^Σ	-0.0041(13)

[70,71]. Plots of the potential energy function and the $\beta(r)$ functions for the $X^2\Sigma^+$ ground state of CaH are displayed in Figs. 2 and 3, respectively.

Selecting ^{40}CaH as the reference isotopologue in our analysis, the effective BOB functions for the hydrogen atom, *i.e.*, $S_{ad}^H(r)$ and $R_{na}^H(r)$, were obtained simultaneously in the fit. We used $p = q = 4$ for these radial strength functions and $q = 4$ for the spin-rotation doubling function, $f_\Sigma(r)$, which is required for $^2\Sigma^+$ states. These functions remain well-behaved outside the data region and display no unphysical behavior. Plots of the adiabatic and nonadiabatic correction functions are presented in Figs. 4-6. As a result, our final multi-isotopologue fit for the radial Hamiltonian of the $X^2\Sigma^+$ ground state required 23 parameters, of which D_e, C_6 and C_8 were held fixed. The fit also included 1886 term values for the excited electronic states. The fitted term values for the $A^2\Pi$ and $B^2\Sigma^+$ states have absolute accuracies of ~0.005 cm^{-1}, and are consistent with spectroscopic constants of CaH and CaD reported previously for these states [30,31]. Table 2 lists the parameters of our final potential function for the $X^2\Sigma^+$ ground state. The sequential rounding and refitting (SRR) technique [68] was applied to

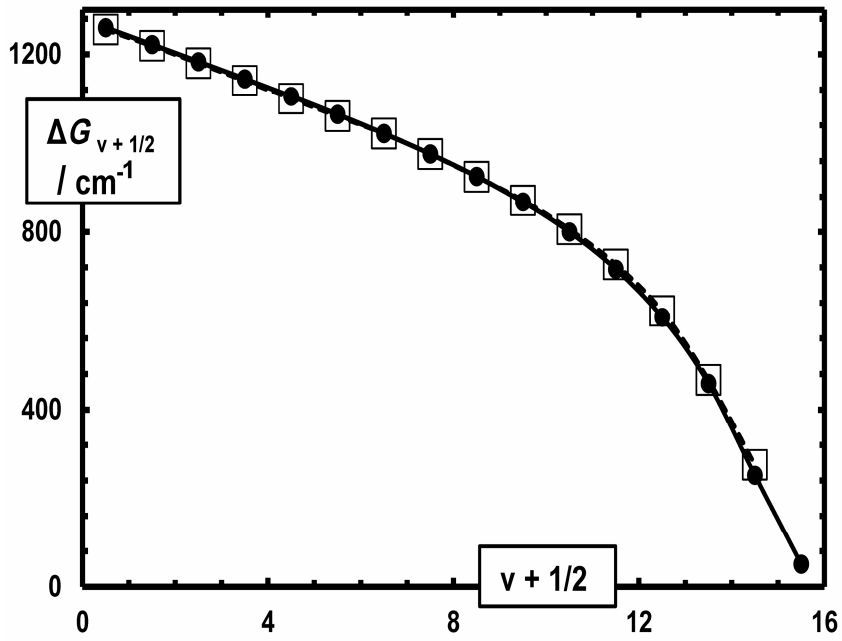

Fig. 7. Vibrational level spacings calculated from the MLR potential function (solid line and circles), compared with those from *ab initio* potential of Ref. [69] (dashed line and squares).

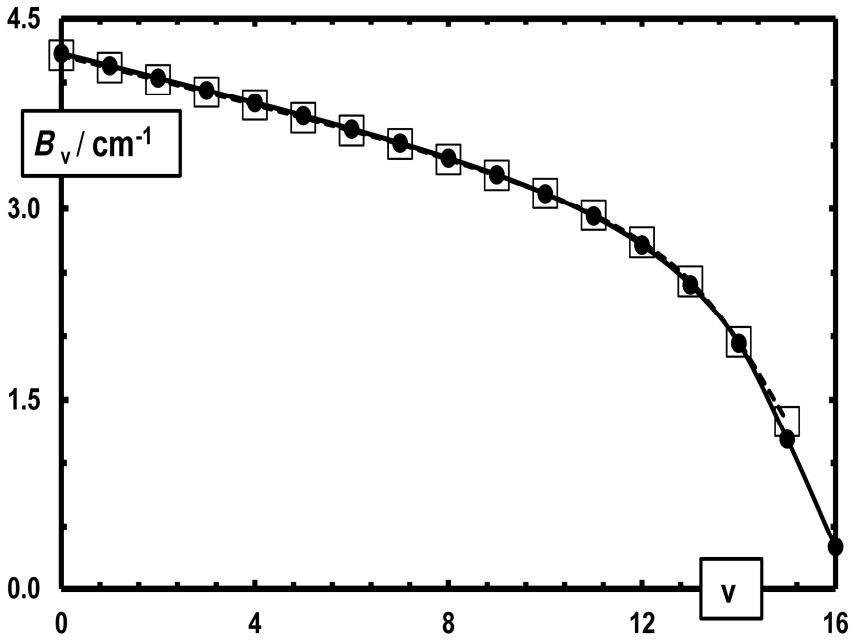

Fig. 8. Rotational constants calculated from the MLR potential function (solid line and circles), compared with those from *ab initio* potential of Ref. [69] (dashed line and squares).

Table 3. Dunham Constants (in cm^{-1}) for the $X^2\Sigma^+$ Ground State of CaH and CaD

Constant	CaH	CaD
$Y_{1,0}$	1298.34461(410)	929.89165(290)
$Y_{2,0}$	-19.1189(48)	-9.8008(25)
$10^2\ Y_{3,0}$	1.206(240)	0.4427(880)
$10^3\ Y_{4,0}$	-2.9(5)	-0.762(140)
$10^4\ Y_{5,0}$	-5.219(450)	-0.9822(850)
$Y_{0,1}$	4.2770402(4)	2.1946977(2)
$10^2 Y_{1,1}$	-9.66232(110)	-3.54842(40)
$10^4 Y_{2,1}$	-1.529(70)	-0.4019(18)
$10^6 Y_{3,1}$	1(2)	0.19(36)
$10^6 Y_{4,1}$	-7.537(180)	-1.016(24)
$10^4\ Y_{0,2}$	-1.852398(160)	-0.4882197(420)
$10^7\ Y_{1,2}$	2.164(180)	0.4073(34)
$10^8\ Y_{2,2}$	2.1(7)	0.283(90)
$10^8\ Y_{3,2}$	-2.546(83)	-0.2456(80)
$10^9\ Y_{0,3}$	6.7706(240)	0.91233(320)
$10^{10}\ Y_{1,3}$	1.01(15)	0.0974(140)
$10^{11}\ Y_{2,3}$	-3.79(23)	-0.262(16)
$10^{13}\ Y_{0,4}$	-3.934(140)	-0.2718(97)
$10^{14}\ Y_{1,4}$	-3.89(41)	-0.192(20)
$10^{17}\ Y_{0,5}$	1.31(24)	0.0464(85)
$10^2\ \gamma_{0,1}$	4.4271(10)	2.2697(5)
$10^3\ \gamma_{1,1}$	-1.404(21)	-0.5154(77)
$10^5\ \gamma_{2,1}$	-1.3(6)	-0.342(140)
$10^6\ \gamma_{0,2}$	-5.039(61)	-1.324(16)
$10^{10}\ \gamma_{0,3}$	2.2(5)	0.296(62)
$\delta^{H}_{1,0}$	0.7276(14)	
$10^3\ \delta^{H}_{2,0}$	3.7(4)	
$10^3\ \delta^{H}_{0,1}$	7.6871(38)	
$10^5\ \delta^{H}_{1,1}$	-8.5(3)	
$10^6\ \delta^{H}_{0,2}$	-1.024(14)	

all the parameters listed in Table 2. A list of term values for the sublevels of the $A^2\Pi$ and $B^2\Sigma^+$ excited states, the outputs of the dPotFit program and a complete list of data with residuals are provided in the supplementary material, in which we also report numerical values of the potential energy function, $V_{MLR}(r)$, and the correction functions $S_{ad}^{H}(r)$, $R_{na}^{H}(r)$ and $f_\Sigma(r)$ at r values from 1.0 Å to 10.0 Å.

Plots of $\Delta G_{v+1/2}$ and B_v of CaH are shown in Figs. 7 and 8, and compared with those from *ab initio* MRCI calculations. On the scale of these plots, the agreement between theory and experiment is excellent. We found the highest vibrational levels of CaH and CaD to be v = 16 and 22, respectively, from the MLR potential. The existence of high-quality millimeter-wave data for both CaH and CaD resulted in accurate determination of the equilibrium internuclear distance (r_e). For three other alkaline earth hydrides, *i.e.*, BeH [72], MgH [58,73] and BaH [74], direct-potential-fit analyses of experimental data have resulted in highly accurate potential energy curves for the $X^2\Sigma^+$ ground state. A similar study on SrH has been completed recently, and will be published separately.

We also performed a multi-isotopologue Dunham fit for the $X^2\Sigma^+$ ground state using the dParFit program [75], while the $A^2\Pi$ and $B^2\Sigma^+$ state levels were fitted as individual term values. We used all the data summarized in Table 1, including the v'' = 5, 6 and 7 of CaD, in our fit. Compared to the Dunham fit reported in Ref. [43], the new fit includes an additional $Y_{5,0}$ parameter, and the $\delta_{3,0}^{H}$ and $\delta_{4,0}^{H}$ correction parameters have been removed. It has been noted previously for other hydride molecules that when higher-order polynomials for $Y_{l,0}$ with fewer correction parameters ($\delta_{l,0}^{H}$) are used in a multi-isotopologue fit, the model is more realistic for predicting higher vibrational intervals [76]. For the rotational part, because we included the $A^2\Pi$-$X^2\Sigma^+$ and $B^2\Sigma^+$-$X^2\Sigma^+$ data with very high J values, we had to add two new parameters, *i.e.*, $Y_{0,5}$ and $\gamma_{0,3}$ to the fit. The r_e value of CaH calculated from the $Y_{0,1}$ constant is 2.0023603(9) Å and the MLR potential has an r_e of 2.0023637(2) Å, the difference being in the sixth decimal place. The zero-point energy, $G(0)$, from the Dunham fit is 644.394 cm^{-1}, and that of the MLR potential is 644.525 cm^{-1}. The $Y_{0,0}$ value of the Dunham fit is 0.131 cm^{-1}, and the two $G(0)$ values become exactly equal when one adds the $Y_{0,0}$ correction. The Dunham constants are listed in Table 3, and the outputs of the dParFit program have been placed in the supplementary material.

CONCLUSIONS

Vibration-rotation and pure rotational data in the $X^2\Sigma^+$ ground state and electronic data from the $A^2\Pi$-$X^2\Sigma^+$ and $B^2\Sigma^+$-$X^2\Sigma^+$ transitions of CaH and CaD were used in the quantum-mechanical direct-potential-fit (DPF) analysis to determine an analytic potential energy function for the $X^2\Sigma^+$ ground state of CaH, and a radial correction function for the CaD isotopologue. This potential energy function reproduces all the observed energy levels of CaH and CaD within their experimental uncertainties and behaves correctly outside the data region.

SUPPLEMENTARY MATERIAL

See supplementary material for a complete list of data and constants.

REFERENCES

[1] Olmstead, C. M., Sun-Spot bands which appear in the spectrum of a calcium arc burning in the presence of hydrogen. *Astrophys. J.* **1908**, *27*, 66-69.

[2] Eagle, A., On the spectra of some of the compounds of the alkaline earths. *Astrophys. J.* **1909**, *30*, 231-236.

[3] Öhman, Y., Spectrographic studies in the red. *Astrophys. J.* **1934**, *80*, 171-180.

[4] Gizis, J. E., M-Subdwarfs: spectroscopic classification and the metallicity scale. *Astronom. J.* **1997**, *113*, 806-822 (1997), DOI: 10.1086/118302.

[5] Lépine, S.; Shara, M. M.; Rich, R. M., Discovery of an ultracool subdwarf: LSR 1425+7102, the first star with spectral type sdM8.0. *Astrophys. J.* **2003**, *585*, L69-L72.

[6] Lépine, S.; Scholz, R. -D., Twenty-three new ultracool subdwarf from the Sloan digital sky survey. *Astrophys. J.* **2008**, *681*, L33-L36.

[7] Mulliken, R. S., A band of unusual structure probably due to a highly unstable calcium hydride molecule.

Phys. Rev. **1925**, *25*, 509-522, DOI: 10.1103/PhysRev.25.509.

[8] Hulthèn, E., On the band spectrum of calcium hydride. *Phys. Rev.* **1927**, *29*, 97-111. DOI: 10.1103/PhysRev.29.97.

[9] Watson, W. W.; Bender, W., The Zeeman effect in the red CaH bands. *Phys. Rev.* **1930**, *35*, 1513-1523, DOI: 10.1103/PhysRev.35.1513.

[10] Watson, W. W., Comparison of the spectra of CaH and CaD. *Phys. Rev.* **1935**, *47*, 27-32, DOI: 10.1103/PhysRev.47.27.

[11] Berg, L. E.; Klynning, L., Rotational analysis of the A -X and B-X band systems of CaH. *Phys. Scr.* **1974**, *10*, 331-336.

[12] Berg, L. E.; Klynning, L., New laboratory measurements of the A2Π-X2Σ and B2Σ-X2Σ transitions of CaH. *Astron. Astrophys. Suppl.* **1974**, *13*, 325-344.

[13] Berg, L. E.; Klynning, L.; Martin, H., Laser excitation spectroscopy of the B2Σ-X2Σ transition of the CaH molecule. *Opt. Commun.* **1976**, *17*, 320-324, DOI: 10.1016/0030-4018(76)90270-4.

[14] Klynning, L.; Martin, H., A doublet state perturbing the A state of CaH. *J. Phys. B: At. Mol. Phys.* **1981**, *14*, L365-L366.

[15] Balfour, W. J.; Klynning, L., On the carrier of the band at 700 nanometers in the iron hydride spectrum of Phillips and Davis: evidence favoring calcium hydride. *Astrophys. J.* **1994**, *424*, 1049-1053.

[16] Huber, K. P.; Herzberg, G., Molecular spectra and molecular structure IV. Constants of diatomic molecules. Van Nostrand, New York, 1979.

[17] Watson, W.; Weber, R., The E band system of calcium hydride. *Phys. Rev.* **1935**, *48*, 732-734, DOI: 10.1103/PhysRev.48.732.

[18] Kaving, B.; Lindgren, B.; Ramsay, D. A., Ultraviolet absorption spectrum of the CaH molecule I. Rotational analysis of the 3060 Å band system. *Phys. Scr.* **1974**, *10*, 73-79.

[19] Kaving, B.; Lindgren, B., Ultraviolet absorption spectrum of the CaH molecule II. The structure of the d-complex around 2800-3200 Å. *Phys. Scr.* **1974**, *10*, 81-85.

[20] Kaving, B.; Lindgren, B., Ultraviolet absorption spectrum of the CaH molecule III. A comparison between CaH and CaD spectra in the region 2800-3200 Å. *Phys. Scr.* **1976**, *13*, 39-46.

[21] Martin, H., Laser spectroscopic investigations of the red band systems of CaH. *J. Mol. Spectrosc.* **1984**, *108*, 66-81, DOI: 10.1016/0022-2852(84)90287-X.

[22] Bell, G. D.; Herman, M.; Johns, J. W. C.; Peck, E. R., The $D^2\Sigma^+$-$X^2\Sigma^+$ band system of CaH. *Phys. Scr.* **1979**, *20*, 609-616.

[23] Gustavsson, T.; Klynning, L.; Lindgren, B., Absorption and emission spectrum of the $D^2\Sigma^+$-$X^2\Sigma^+$ transition of the CaD molecule. *Phys. Scr.* **1985**, *31*, 269−274.

[24] Martin, H., Empirically fitting the potential energy curves for the X, B, and B′ double minimum and the D2Σ+ states in CaH using united knowledge of CaH and CaD. *J. Chem. Phys.* **1988**, *88*, 1797-1806, DOI: 10.1063/1.454103.

[25] Ram, R. S.; Tereszchuk, K.; Gordon, I. E.; Walker, K. A.; Bernath, P. F., Fourier transform emission spectroscopy of the $E^2\Pi$-$X^2\Sigma^+$ transition of CaH and CaD. *J. Mol. Spectrosc.* **2011**, *266*, 86-91, DOI: 10.1016/j.jms.2011.03.009.

[26] Steimle, T. C.; Gengler, J.; Chen, J., A study of the $A^2\Pi$-$X^2\Sigma^+$ band systems of calcium monohydride (CaH) using a supersonic molecular beam source and laser-induced fluorescence detection. *Can. J. Chem.* **2004**, *82*, 779-790, DOI: 10.1139/v04-077.

[27] Chen, J.; Gengler, J.; Steimle, T. C.; Brown, J. M, Optical Zeeman spectroscopy of calcium monohydride. *J. M. Phys. Rev. A.* **2006**, *73*, 012502-012509, DOI: 10.1103/PhysRevA.73.012502.

[28] Steimle, T. C.; Chen, J. J.; Gengler, J., The permanent electric dipole moments of calcium monohydride, CaH. *J. Chem. Phys.* **2004**, *121*, 829-834, 10.1063/1.1759314.

[29] Chen, J.; Steimle, T. C., The permanent electric dipole moment of calcium monodeuteride. *J. Chem. Phys.* **2008**, *128*, 144312-144318. DOI: 10.1063/1.2899651.

[30] Shayesteh, A.; Ram, R. S.; Bernath, P. F., Fourier transform emission spectra of the $A^2\Pi \rightarrow X^2\Sigma^+$ and $B^2\Sigma^+ \rightarrow X^2\Sigma^+$ band systems of CaH, *J. Mol. Spectrosc.* **2013**, *288*, 46-51, DOI: 10.1016/j.jms.2013.04.009.

[31] GharibNezhad, E.; Shayesteh, A.; Bernath, P. F., Fourier transform emission spectra of the $A^2\Pi \rightarrow X^2\Sigma^+$ and $B^2\Sigma^+ \rightarrow X^2\Sigma^+$ transitions of CaD. *J. Mol. Spectrosc.* 2012, *281*, 47-50, DOI: 10.1016/j.jms.2012.10.001.

[32] Watanabe, K.; Yoneyama, N.; Uchida, K.; Kobayashi, K.; Matsushima, F.; Moriwaki, Y.; Ross, S.C., According theory and experiment in CaH: laser-induced fluorescence study of new B/B′-X bands in the UV region. *Chem. Phys. Lett.* **2016**, *657*, 1-7, DOI: 10.1016/j.cplett.2016.05.033.

[33] Jeung, G.; Daudey, J. -P.; Malrieu, J. -P., Theoretical study of the electronic states of calcium and calcium hydride. *Chem. Phys. Lett.* **1983**, *98*, 433-438, DOI: 10.1016/0009-2614(83)80082-7.

[34] Pettersson, L. G. M.; Siegbahn, P. E. M.; Ismail, S., Core-valence correlation effects in calcium hydride. *Chem. Phys.* **1983**, *82*, 355-368, DOI: 10.1016/0301-0104(83)85240-9.

[35] Fuentealba, P.; Reyes, O.; Stoll, H.; Preuss, H., Ground state properties of alkali and alkaline-earth hydrides. *J. Chem. Phys.* **1987**, *87*, 5338-5338, DOI: 10.1063/1.453653.

[36] Boutalib, A.; Daudey, J. P.; Mouhtadi, M. El, Theoretical study of the lowest electronic states of CaH and CaH^+ molecules. *Chem. Phys.* **1992**, *167*, 111-120, DOI: 10.1016/0301-0104(92)80026-R.

[37] Leininger, T.; Jeung, G. -H., *Ab initio* calculation of rovibronic transition spectra of CaH. *J. Chem. Phys.* **1995**, *103*, 3942-3942, DOI: 10.1063/1.469581.

[38] Holka, F.; Urban, M., The dipole moment and molecular properties of CaH: a theoretical study. *Chem. Phys. Lett.* **2006**, *426*, 252-256, DOI: 10.1016/j.cplett.2006.05.108.

[39] Kerkines, I. S. K.; Mavridis, A., A theoretical study of calcium monohydride, CaH: low-lying states and their permanent electric dipole moments. *J. Phys. Chem. A.* **2007**, *111*, 371-374, DOI: 10.1021/jp064705k.

[40] Weck, P. F.; Stancil, P. C.; Kirby, K., Theoretical study of the rovibrationally resolved transitions of CaH. *J. Chem. Phys.* **2003**, *118*, 9997-10005, DOI: 10.1063/1.1573181.

[41] Petitprez, D.; Lemoine, B.; Demuynck, C.; Destombes, J. L.; Macke, B., Infrared diode laser spectroscopy of CaH and CaD (X2Σ+): determination of mass-independent parameters. *J. Chem. Phys.* **1989**, *91*, 4462-4467, DOI: http://dx.doi.org/10.1063/1.456783.

[42] Frum, C. I.; Pickett, H. M., High-resolution infrared Fourier transform emission spectroscopy of metal hydrides: $X^2\Sigma^+$ state of CaH, *J. Mol. Spectrosc.* **1993**, *159*, 329-336, DOI: 10.1006/jmsp.1993.1130.

[43] Shayesteh, A.; Walker, K. A.; Gordon, I.; Appadoo, D. R. T.; Bernath, P. F., New Fourier transform infrared emission spectra of CaH and SrH: combined isotopomer analyses with CaD and SrD. *J. Mol. Struct.* **2004**, *695/696*, 23-37, DOI: 10.1016/j.molstruc.2003.11.001.

[44] Barclay, Jr.; W. L.; Anderson, M. A.; Ziurys, L. M., The millimeter-wave spectrum of CaH ($X^2\Sigma^+$), *Astrophys. J.* **1993**, *408*, L65-L67.

[45] Frum, C. I.; Oh, J. J.; Cohen, E. A.; Pickett, H. M., Rotational spectra of the $X^2\Sigma^+$ states of CaH and CaD. *Astrophys. J.* **1993**, *408*, L61-L61.

[46] Herman, R. M.; Asgharian, A., Theory of energy shifts associated with deviations from Born-Oppenheimer behavior in $1\Sigma^+$-state diatomic molecules. *J. Mol. Spectrosc.* **1966**, *19*, 305-324, DOI: 10.1016/0022-2852(66)90254-2.

[47] Bunker, P. R.; Moss, R. E, The breakdown of the Born-Oppenheimer approximation: the effective vibration-rotation Hamiltonian for a diatomic molecule. *Mol. Phys.* **1977**, *33*, 417-424, DOI: 10.1080/00268977700100351.

[48] Herman, R. M.; Ogilvie, J. F., An effective Hamiltonian to treat adiabatic and nonadiabatic effects in the rotational and vibrational spectra of diatomic molecules. *Adv. Chem. Phys.* **1998**, *103*, 187-215.

[49] Coxon, J. A.; Hajigeorgiou, P. G., The radial Hamiltonians for the $X1\Sigma^+$ and $B1\Sigma^+$ states of HCl. *J. Mol. Spectrosc.* **2000**, *203*, 49-64, DOI: 10.1006/jmsp.2000.8155.

[50] Rey, M.; Tyuterev, V. G.; Coxon, J.; Le Roy, A. R. J., Resolution of a convergence problem in direct-potential-fit data analyses: applications to GaH ($X1\Sigma^+$) and ArH^+ ($X1\Sigma^+$). *J. Mol. Spectrosc.* **2006**, *238*, 260-263, DOI: 10.1016/j.jms.2006.05.006.

[51] Watson, J. K. G., The isotope dependence of diatomic

Dunham coefficients. *J. Mol. Spectrosc.* **1980**, *80*, 411-421. DOI: 10.1016/0022-2852(80)90152-6.

[52] Le Roy, R. J., Algebraic *vs.* numerical methods for analysing diatomic spectral data: a resolution of discrepancies. *J. Mol. Spectrosc.* **2004**, *228*, 92–104, DOI: 10.1016/j.jms.2004.03.022.

[53] Le Roy, R. J., Improved parameterization for combined isotopomer analysis of diatomic spectra and its application to HF and DF. *J. Mol. Spectrosc.* **1999**, *194*, 189-196, DOI: 10.1006/jmsp.1998.7786.

[54] Le Roy, R. J.; Huang, Y, Representing Born–Oppenheimer breakdown radial correction functions for diatomic molecules. *J. Mol. Struct: THEOCHEM.* **2002**, *591*, 175-187, DOI: 10.1016/S0166-1280(02)00239-7.

[55] Watson, J. K. G., The inversion of diatomic Born-Oppenheimer-breakdown corrections, *J. Mol. Spectrosc.* 2004, *223*, 39-50, DOI: 10.1016/j.jms.2003.09.007.

[56] Dattani, N. S.; Le Roy, R. J., State of the art for *ab initio vs.* empirical potentials for predicting 6e-excited state molecular energies: application to Li2 (b, 13Πu). 2015, https://arxiv.org/pdf/1508.07184.pdf

[57] Le Roy, R. J., dPotFit: a computer program to fit diatomic molecule spectral data to potential energy functions. *J. Quant. Spectrosc. Radiat. Transfer.* **2017**, *186*, 179-196, DOI: 10.1016/j.jqsrt.2016.06.002.

[58] Henderson, R. D. E.; Shayesteh, A.; Tao, J.; Haugen, C. C.; Bernath, P. F.; Le Roy, R. J., Accurate analytic potential and Born-Oppenheimer breakdown functions for MgH and MgD from a direct-potential-fit data analysis, *J. Phys. Chem. A*. **2013**, *117*, 13373-13387, DOI: 10.1021/jp406680r.

[59] Le Roy, R. J.; Huang Y.; Jary, C., An accurate analytic potential function for ground-state N2 from a direct-potential-fit analysis of spectroscopic data. *J. Chem. Phys.* **2006**, *125*, 164310-164322, DOI: 10.1063/1.2354502.

[60] Le Roy, R. J.; Dattani, N. S.; Coxon, J. A.; Ross, A. J.; Crozet, P.; Linton, C., Accurate analytic potentials for Li2 ($X^1\Sigma_g^+$) and Li2 ($A^1\Sigma_u^+$) from 2 to 90 Å, and the radiative lifetime of Li(2p). *J. Chem. Phys.* **2009**, *131*, 204309-204329, DOI: 10.1063/1.3264688.

[61] Šurkus, A. A.; Rakauskas, R. J.; Bolotin, A. B., The generalized potential energy function for diatomic molecules. *Chem. Phys. Lett.* 1984, *105*, 291–294, DOI: 10.1016/0009-2614(84)85032-0.

[62] Dattani, N. S.; Le Roy, R. J., A DPF data analysis yields accurate analytic potentials for Li2($a^3\Sigma_u^+$) and Li2($1^3\Sigma_g^+$) that incorporate 3-state mixing near the $1^3\Sigma_g^+$ state asymptote. *J. Mol. Spectrosc.* **2011**, *268*, 199-210, DOI: 10.1016/j.jms.2011.03.030.

[63] Le Roy, R. J.; Haugen, C. C.; Tao, J.; Li, H., Long-range damping functions improve the short-range behaviour of 'MLR' potential energy functions. *Mol. Phys.* **2011**, *109*, 435-446, DOI: 10.1080/00268976.2010.527304.

[64] Douketis, C.; Scoles, G.; Marchetti, S.; Zen, M.; Thakkar, A.J., Intermolecular forces *via* hybrid Hartree-Fock-SCF plus damped dispersion (HFD) energy calculations. An improved spherical model. *J. Chem. Phys.* **1982**, *76*, 3057-3063, DOI: 10.1063/1.443345.

[65] Mitroy, J.; Zhang, J. -Y., Properties and long range interactions of the calcium atom. *J. Chem. Phys.* **2008**, *128*, 134305-134317, DOI: 10.1063/1.2841470.

[66] Le Roy, R. J., RKR1: a computer program implementing the first-order RKR method for determining diatomic molecule potential energy functions. *J. Quant. Spectrosc. Radiat. Transfer.* **2017**, *186*, 158-166, DOI: 10.1016/j.jqsrt.2016.03.030.

[67] Le Roy, R. J., betaFIT: a computer program to fit pointwise potentials to selected analytic functions. *J. Quant. Spectrosc. Radiat. Transfer.* **2017**, *186*, 210-220, DOI: 10.1016/j.jqsrt.2016.03.036.

[68] Le Roy, R. J., Uncertainty, sensitivity, convergence, and rounding in performing and reporting least-squares fits. *J. Mol. Spectrosc.* **1998**, *191*, 223-231, DOI: 10.1006/jmsp.1998.7646.

[69] Shayesteh, A.; Alavi, S. F.; Rahman, M.; Gharib-Nezhad, E., *Ab initio* transition dipole moments and potential energy curves for the low-lying electronic states of CaH. *Chem. Phys. Lett.* **2017**, *667*, 345-350, DOI: 10.1016/j.cplett.2016.11.020.

[70] Cho, Y. -S.; Le Roy, R. J., Full empirical potential curves for the $X1\Sigma^+$ and $A1\Pi$ states of CH^+ from a direct-potential-fit analysis. *J. Chem. Phys.* **2016**, *144*, 024311-024323, DOI: 10.1063/1.4939274.

[71] Shayesteh, A.; Ghazizadeh, E., Analytic potential energy functions for the $X1\Sigma^+$ and $a^3\Pi0^+$ states of InH from a direct-potential-fit data analysis. *J. Mol. Spectrosc.* **2016**, *330*, 72-79, DOI: 10.1016/ j.jms.2016.07.013.

[72] Dattani, N. S., Beryllium monohydride (BeH): Where we are now, after 86 years of spectroscopy. *J. Mol. Spectrosc.* **2015**, *311*, 76-83, DOI: 10.1016/ j.jms.2014.09.005.

[73] Shayesteh, A.; Henderson, R. D. E.; Le Roy, R. J.; Bernath, P.F., Ground state potential energy curve and dissociation energy of MgH, *J. Phys. Chem. A.* **2007**, *111*, 12495-12505, DOI: 10.1021/jp075704a.

[74] Moore, K.; McLaughlin, B. M.; Lane I. C., Towards a spectroscopically accurate set of potentials for heavy hydride laser cooling candidates: effective core potential calculations of BaH. *J. Chem. Phys.* **2016**, *144*, 144314-144325, DOI: 10.1063/1.4945623.

[75] Le Roy, R. J., dParFit: a computer program for fitting diatomic molecule spectral data to parameterized level energy expressions. *J. Quant. Spectrosc. Radiat. Transfer.* **2017**, *186*, 197-209, DOI: 10.1016/ j.jqsrt.2016.04.004.

[76] Shayesteh, A.; Le Roy, R. J.; Varberg, T. D.; Bernath, P. F., Multi-isotopologue analyses of new vibration-rotation and pure rotation spectra of ZnH and CdH. *J. Mol. Spectrosc.* **2006**, *237*, 87-96, DOI: 10.1016/ j.jms.2006.03.004.